Conduction electrons mediating the evolution from antiferromagnetic to ferromagnetic ordering in $Gd(Co_{1-y}Fe_y)_2Zn_{20}$ ($0 \leqslant y \leqslant 1$)

M. Cabrera-Baez,[1,*] A. Naranjo-Uribe,[2] J. M. Osorio-Guillén,[2] C. Rettori,[1,3] and M. A. Avila[1,†]

[1]*CCNH, Universidade Federal do ABC (UFABC), Santo André, SP 09210-580, Brazil*

[2]*Instituto de Física, Universidad de Antioquia UdeA, Calle 70 No. 52-21, Medellín, Colombia*

[3]*Instituto de Física "Gleb Wataghin," UNICAMP, Campinas, SP 13083-859, Brazil*

(Received 9 December 2016; published 8 March 2017)

$GdFe_2Zn_{20}$ is a complex cagelike compound with an unusually high ferromagnetic ordering temperature ($T_C = 86$ K) for a very diluted Gd^{3+} magnetic sublattice, embedded in a matrix that features strong electron-electron correlations. Here, we report on a magnetic and electronic study of the substitutional intermetallic system $Gd(Co_{1-y}Fe_y)_2Zn_{20}$ combining magnetization measurements plus first-principles density functional theory (DFT) calculations with temperature-dependent electron spin resonance (ESR). After accounting for electron-electron correlations and itinerant molecular field effects, the ESR results indicate that the exchange interaction between the Gd^{3+} is processed via a single band of d-type electrons at the Fermi level and the exchange interaction is covalent in nature [$J(0)_{fd} < 0$] with a strong conduction electron (ce) momentum transfer dependence [$J_{fd}(q)$]. The DFT calculations support this scenario by indicating a major contribution of d-type ce at the Fermi level and a spin polarization in $(Y,Gd)Fe_2Zn_{20}$ wherein the most stable configuration is antiferromagnetic between Gd^{3+} and ce spins. Our results demonstrate that the standard Ruderman-Kittel-Kasuya-Yosida mechanism cannot explain the ferromagnetic behavior of $GdFe_2Zn_{20}$ and a superexchangelike mechanism is proposed for this magnetic interaction. An "extended phase diagram" for the double substitution sequence $YCo_2Zn_{20} \rightarrow GdCo_2Zn_{20} \rightarrow GdFe_2Zn_{20}$ is presented and discussed.

DOI: 10.1103/PhysRevB.95.104407

I. INTRODUCTION

Unconventional ferromagnetic behaviors are occasionally seen in nature, especially in materials with complex structures [1]. The magnetic interactions manifested in systems with a large separation between rare-earth ions (naturally diluted magnetic systems) are interesting toy models in materials physics because they allow clean analyses and can provide opportunities to simplify the complexity of the involved magnetic orders. The exchange interaction between the rare-earth ion ($4f$ local magnetic moments) and uncorrelated conduction electrons (ce) leads to magnetic order via the well-known Rutterman-Kittel-Kasuya-Yosida (RKKY) mechanism for these distant lattice-site systems [2–4]. However, for certain types of materials with d-type ce at the Fermi level, the involved interaction can be enriched by the presence of ce electron-electron correlations [5]. Generally, this type of material, often referred to as nearly ferromagnetic Fermi liquids (NFFLs), is close to the Stoner limit and manifests an enhanced T-dependent Pauli paramagnetic susceptibility [6–9]. When a localized magnetic moment is embedded in this kind of NFFL matrix, the magnetic response is that of polarized correlated ce that can account for high values of ordering temperatures [7].

An example of a very dilute rare-earth system is the family of RT_2Zn_{20} (R = rare earth, T = transition metal) [10] in which recent studies showed that for T = Fe, Ru, Os and R = Gd the compounds present ferromagnetic (FM) ground states, whereas for T = Co, Rh, Ir and R = Gd, the compounds show antiferromagnetic (AFM) order [8]. In the case of Gd^{3+} localized magnetic moments in the uncorrelated ce matrix of $GdCo_2Zn_{20}$, we have recently shown that the AFM order is accounted for by the RKKY interaction [4]. When the same localized magnetic moment is embedded in a correlated ce system, as in $GdFe_2Zn_{20}$ lying near the Stoner limit, the system becomes FM and the RKKY interaction might not describe the FM order due to the strong correlation between the ce (spin polarization) [9].

The deviation of the inverse dc magnetic susceptibility from the high-T linear behavior in $GdFe_2Zn_{20}$ has raised the prospect that this may represent a peculiar type of FM order [9]. The scenario suggested by the authors, involving the formation of magnetic droplets above T_C which consist of Gd^{3+} local moments and a cloud of oppositely and highly polarized ce, was contradicted by subsequent results from Mössbauer experiments [11] which reported the absence of a hyperfine field on the ^{57}Fe site above $T \approx 90$ K. Thus, further investigation is needed to clarify the issue.

With this in mind, we have now performed T-dependent electron spin resonance (ESR) and magnetization experiments combined with density functional theory (DFT) calculations on YFe_2Zn_{20} and on the pseudoquaternary system $Gd(Co_{1-y}Fe_y)Zn_{20}$, which evolves continuously from uncorrelated to correlated ce for $0 \leqslant y \leqslant 1$. In YFe_2Zn_{20} our DFT calculations show a major contribution of polarized d-like ce (spin up) at the Fermi level, in agreement with reported results [8]. In $GdFe_2Zn_{20}$ the polarization of the d-like ce decreases slightly and shows a minimized energy configuration for the case of opposite coupling with the Gd^{3+} $4f$ electrons (spin down). Moreover, our ESR results above T_C show that there is a negative microscopic exchange coupling parameter ($J_{fd} < 0$) between the Gd^{3+} $4f$ electron and Fe d-like ce, consistent

*michael.cabrera@ufabc.edu.br

†avila@ufabc.edu.br

with the DFT. The combined results support a scenario where, in the paramagnetic regime, a cloud of polarized d-like ce is coupled to the Gd^{3+} $4f$ electrons but in the opposite direction.

An additional and relevant ESR result obtained for $GdFe_2Zn_{20}$ is a ce momentum transfer dependence (q dependence) of the exchange interaction [12] $J_{fd}(q)$. This is evidenced by the difference between the average of the exchange interaction over the Fermi surface (involving relaxation processes) as compared to the zero momentum transfer exchange parameter (involving polarization effects), i.e., $\langle J_{fd}(q)\rangle_F \neq J_{fd}(0)$, suggesting a significant change in the Fermi surface of this compound [13] due to the ce polarization when compared with the Fermi surfaces of unpolarized ce in $GdCo_2Zn_{20}$ [4].

Finally, we discuss the general evolution of the local moment coupling mechanisms as viewed by the ESR parameters of Gd^{3+} in the generalized system $Y_{1-x}Gd_x(Co_{1-y}Fe_y)_2Zn_{20}$ for ($0 \leqslant x \leqslant 1$, $y = 0$) and ($x = 1$, $0 \leqslant y \leqslant 1$), going from the Pauli-like paramagnetism of $Y_{1-x}Gd_xCo_2Zn_{20}$ to the AFM of $GdCo_2Zn_{20}$ and finally to the FM of $GdFe_2Zn_{20}$.

II. EXPERIMENTAL AND COMPUTATIONAL DETAILS

Several batches of $Gd(Co_{1-y}Fe_y)_2Zn_{20}$ ($0 \lesssim y \leqslant 1$) single crystals were grown by the standard self-flux method [14,15] using an excess of Zn. The constituent elements were 99.9% Gd, 99.9% Fe, 99.9% Co, and 99.9999% Zn (Alfa-Aesar). The initial ratios of the elements were 1 : 2 : 47 for the pure ternaries Gd:Co:Zn and Gd:Fe:Zn, and $1 : 2 - y : y : 47$ for the pseudoquaternaries Gd:Fe:Co:Zn. The initial reagents were sealed in an evacuated quartz ampoule and heated in a box furnace. Crystals were grown by slowly cooling the melt between 1100 and 600 °C over 100 h. At 600 °C the ampoules were removed from the furnace, inverted, and placed in a centrifuge to spin off the excess flux, following previous reports [8]. The Fe and Co concentrations for all of our samples were evaluated using energy dispersive x-ray spectroscopy (EDS) measurements on a JEOL model JSM-6010LA with a Vantage EDS system. The effective amounts of Fe and Co thus obtained are in very good agreement with the nominal compositions of each sample. X-ray powder diffraction of crushed crystals at room temperature was carried out to verify the $CeCr_2Al_{20}$-type structure [10] and found to agree with previous published data [7]. Magnetic susceptibility ($\chi = M/H$) measurements were conducted on a Quantum Design MPMS3-SQUID magnetometer at various applied magnetic fields ($H \leqslant 3$ T) and temperatures ($2.0\ \text{K} \leqslant T \leqslant 310$ K). For the ESR experiments, single crystals were crushed into fine powders of particle size greater than 100 μm, corresponding to average grain size (d) being larger than the skin depth (δ), $\lambda = d/\delta \gtrsim 10$. The X-band ($\nu \approx 9.4$ GHz) ESR experiments were performed on a conventional cw Bruker-ELEXSYS 500 ESR spectrometer using a TE_{102} cavity. The sample temperature was changed using a helium gas-flux system coupled to an Oxford temperature controller.

The calculation details are as follows: The ground state crystal structures were calculated using spin-polarized first-principles DFT, the Kohn-Sham equations were solved by the projector augmented plane-wave (PAW) method as implemented within the VASP code [16,17], and we used the semilocal Perdew-Burke-Ernzerhof (PBEsol) exchange-correlation functional [18]. Atomic valence configurations used in the PAW potentials were $5s^25p^64f^75d^16s^2$ for Gd, $3s^23p^63d^64s^2$ for Fe, $3s^23p^63d^74s^2$ for Co, and $3p^63d^{10}4s^2$ for Zn. The cutoff energy for the basis set was set at 507.7 eV and 400 bands were used. An energy convergence of 1 meV/unit cell and an ionic-force convergence of 0.1 meV/Å were achieved using the conjugated-gradient algorithm, allowing full cell relaxation (ionic positions and unit cell shape and volume). A Monkhorst-Pack $12 \times 12 \times 12$ **k** mesh was used during the relaxation. After structure relaxation, calculations of the total and partial density of states (DOS) were done using a Γ-centered $20 \times 20 \times 20$ **k** mesh.

III. EXPERIMENTAL AND COMPUTATIONAL RESULTS

Figure 1(a) displays the Gd^{3+} ESR spectrum in $GdFe_2Zn_{20}$ at $T = 90$ K and microwave power of $P_{\mu\omega} \approx 2$ mW. This ESR spectrum presents a different resonance magnetic field than that of Gd^{3+} in insulators, $H_0 = 3386(4)$ Oe with $g_0 = 1.993(2)$ [19]. It is evident that this resonance is shifted ($\Delta g_{\text{eff}} = g_{\text{eff}} - g_0$) toward a higher field (lower g value). The

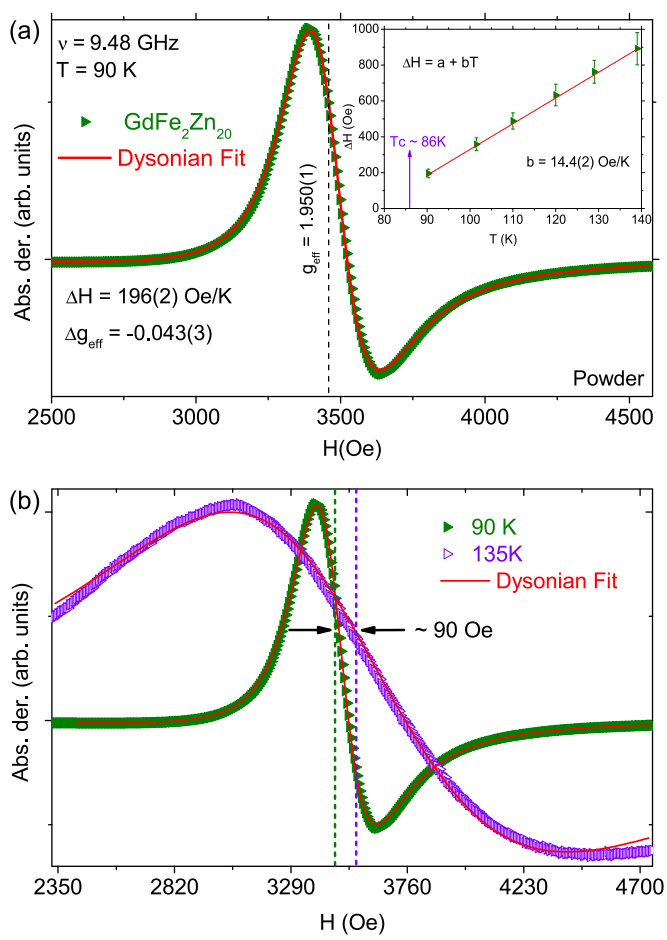

FIG. 1. (a) Gd^{3+} ESR spectra of $GdFe_2Zn_{20}$ at $T = 90$ K for a microwave power of $P_{\mu\omega} \approx 2$ mW. The inset shows the linewidth as a function of T showing a Korringa-like relaxation of $b = 14.4(2)$ Oe/K. (b) Gd^{3+} ESR spectra of $GdFe_2Zn_{20}$ at $T = 90$ and 135 K showing an extra contribution of the g shift.

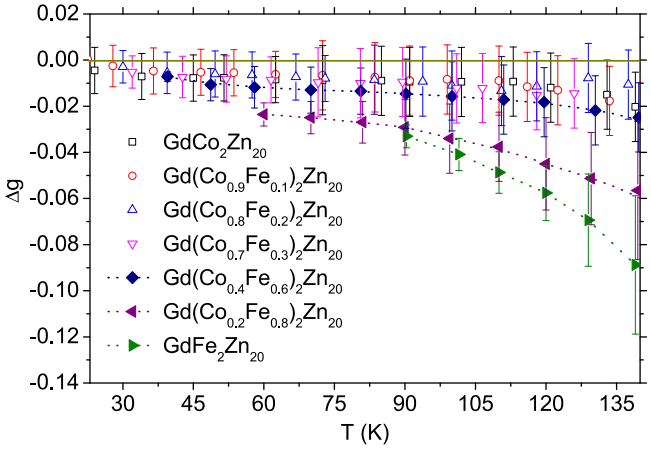

FIG. 2. Fe concentration (y) dependence of the g shift [$\Delta g_{\rm eff} = g_{\rm eff} - 1.993(2)$] vs T for the $Gd(Co_{1-y}Fe_y)_2Zn_{20}$ system. The dashed lines are guides for the eye.

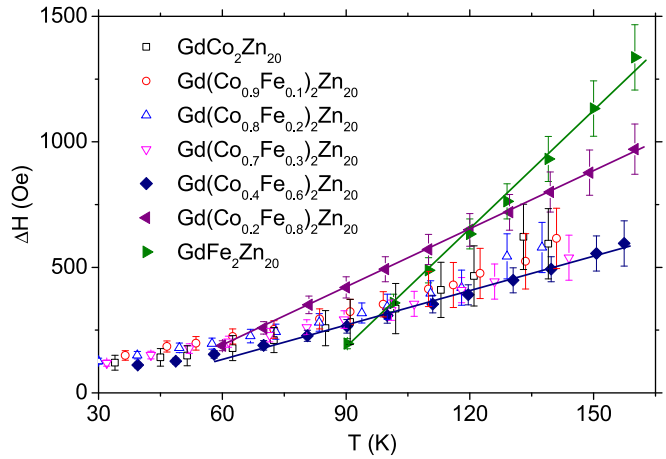

FIG. 3. T dependence of the Gd^{3+} ESR linewidth ΔH in $Gd(Co_{1-y}Fe_y)_2Zn_{20}$ for $0 \leqslant y \leqslant 1$. The solid lines are the high-T linear fittings.

inset shows the linear thermal broadening of the linewidth ΔH with a slope of $b = d(\Delta H)/dT = 14.4(2)$ Oe/K. The observed ESR spectra of the Gd^{3+} localized magnetic moments in $Gd(Co_{1-y}Fe_y)_2Zn_{20}$ will be analyzed in terms of the Dyson theory [20,21]. Following the same procedure employed in our previous works [4,22], we extract the two most relevant ESR parameters, i.e., the g value from the resonance condition $h\nu = g\mu_B H_r$, and the linewidth ΔH (see Fig. 1). Figure 1(b) shows the Gd^{3+} ESR spectra at two different temperatures (90 K in green and 135 K in purple) showing a T-dependent resonance field, 3550 Oe at high temperatures and 3460 Oe just above T_C, for this ferromagnetic material.

Figure 2 displays the Fe concentration (y) and T dependence of the g shift [$\Delta g_{\rm eff} = g_{\rm eff} - 1.993(2)$] in the system $Gd(Co_{1-y}Fe_y)_2Zn_{20}$. A pronounced T dependence of the g shift is observed for Fe concentrations above $y \gtrsim 0.3$, suggesting, above this value, a percolated magnetic of the Fe $3d$ wave function. For all samples the trends of the data in Fig. 2 show increasing negative g shifts that evolve to even higher values as the samples become more strongly FM.

Figure 3 displays the T dependence of the Gd^{3+} ESR linewidth ΔH in $Gd(Co_{1-y}Fe_y)_2Zn_{20}$ for $0 \leqslant y \leqslant 1$. The high-$T$ dependence of ΔH follows a linear behavior $\Delta H = a + bT$, where a represents the residual linewidth ΔH_0 and $b = d(\Delta H)/dT$ is the Korringa-like relaxation rate. The extracted b values are given in Table I, together with the corresponding g shifts at low T (just above T_C) and high T (140–160 K before the loss of the ESR signal).

Figure 4 presents the T dependence of the $GdFe_2Zn_{20}$ inverse dc magnetic susceptibility measured at 1000 Oe. A high-T, Curie-Weiss fitting (Fig. 4) leads to an effective magnetic moment of $\mu_{\rm eff} \approx 8.0(1)\mu_B$, appropriate for Gd^{3+} ions ($\mu_{\rm eff} = 7.94\mu_B$), and a paramagnetic Curie temperature $\theta_C \approx 56$ K, in agreement with published results [8]. The inset of Fig. 4 shows the dc magnetic susceptibility for YFe_2Zn_{20} measured at 3460 Oe.

Figure 5(a) shows the band structure results of our DFT calculations, giving polarized total and partial density of states for YFe_2Zn_{20} and $GdFe_2Zn_{20}$. There is a strong contribution of d-like ce at the Fermi level which is mainly associated with the Fe ions [Fig. 5(b)], in agreement with previous results [8]. In the case of $GdFe_2Zn_{20}$ there is also a polarized total and partial density of states with a strong contribution of d-like ce at the Fermi level, but opposite to the Gd^{3+} $4f$ electrons [Fig. 5 b). These results, summarized in Table II, are also consistent with reported work using the tight-binding linear muffin-tin orbital method and the atomic sphere approximation [8,23]. Some differences appear in the shape of the DOS due mainly to our dense **k**-point mesh (256 irreducible **k** points) compared to 16 irreducible **k** points of the other calculations [8,23].

IV. ANALYSIS AND DISCUSSION

Figure 1 shows the Gd^{3+} ESR spectrum of $GdFe_2Zn_{20}$ at $T = 90$ K (above $T_C = 86$ K) with a $\Delta g_{\rm eff} = -0.043(3)$ and a Korringa parameter $b = 14.4(7)$ Oe/K. In the usual ESR analysis these two quantities are T independent and directly connected via the exchange coupling between the Gd^{3+} localized magnetic moment and the host ce [22]. However, for samples with $y = 0.6$, 0.8, and 1.0, the Δg in the region $T > T_C$ (Fig. 2) shows a considerable T dependence. This is presumably associated with a T-dependent AFM molecular-like internal magnetic field, $H_{\rm AFM} = \lambda M_d$ in the paramagnetic region, possibly due to an enhanced T-dependent magnetic

TABLE I. Fe concentrations (y), g-shift values at low and high T, and thermal broadening of the linewidths b for the $Gd(Co_{1-y}Fe_y)_2Zn_{20}$ system.

Conc. y	Δg (low T)	Δg (high T)	b (Oe/K)
0.0	− 0.002(2)	− 0.008(5)	2.2(4)
0.1	− 0.002(3)	− 0.009(5)	2.2(4)
0.2	− 0.002(2)	− 0.011(5)	2.2(4)
0.3	− 0.003(2)	− 0.023(4)	2.3(4)
0.6	− 0.007(2)	− 0.039(4)	3.7(7)
0.8	− 0.0024(2)	− 0.08(4)	7.8(7)
1.0	− 0.043(2)	− 0.13(4)	14.4(7)

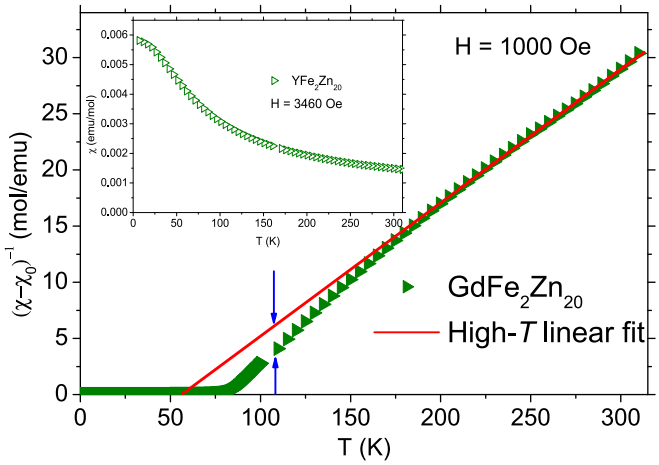

FIG. 4. Inverse magnetic susceptibility as a function of temperature. The red line is a linear fitting at high T. The inset shows the direct susceptibility for YFe_2Zn_{20} at $H = 3460$ Oe.

susceptibility of the host itinerant (mainly d-like) ce, $M_d = \chi_d H$. This behavior contrasts with that of the AFM $GdCo_2Zn_{20}$

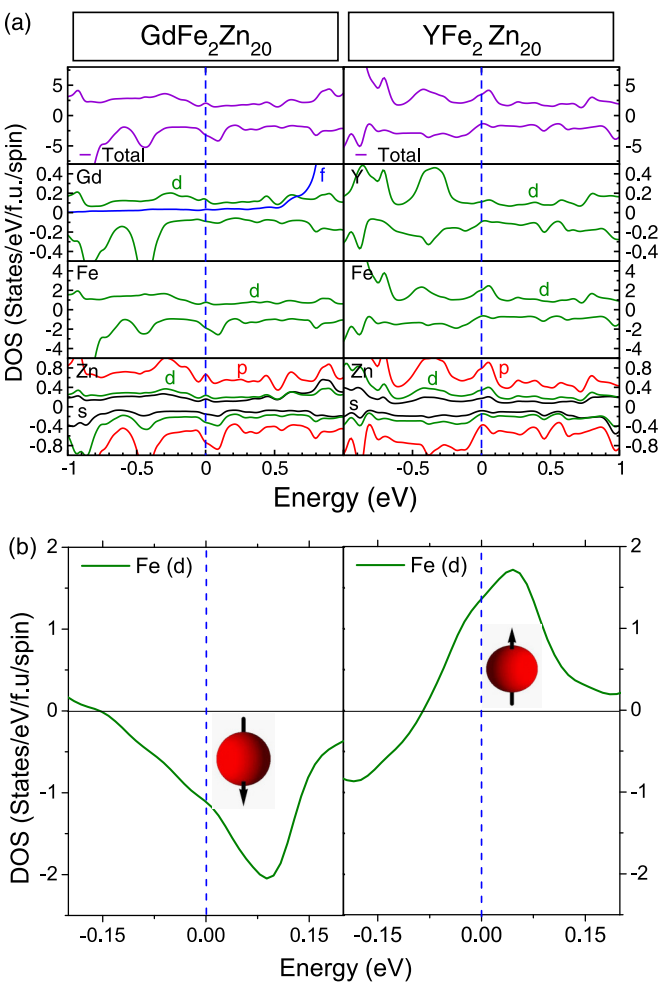

FIG. 5. (a) Calculated total and partial DOS for $GdFe_2Zn_{20}$ and YFe_2Zn_{20}. (b) Partial DOS sum of the spin up and spin down for the d-type ce for $GdFe_2Zn_{20}$ and YFe_2Zn_{20}. The Fermi level is indicated by a dashed line.

($y = 0$) in the paramagnetic region, where Δg is basically T independent (see Fig. 2) and the canonical ESR analysis of the data could be applied [4]. Therefore, the analysis of the ESR data for $GdFe_2Zn_{20}$ has to take into account the AFM internal field before the proper intrinsic parameters associated with the Gd^{3+} ESR data in $GdFe_2Zn_{20}$ can be extracted.

Figure 4 shows the T dependence of the inverse magnetic susceptibility for $GdFe_2Zn_{20}$ and the straight red line corresponds to the high-T fitting (250–310 K) to the Curie-Weiss law. These data show that below $T \approx 200$ K there is an *extra* enhancement of susceptibility, beyond that of the high-T Curie-Weiss behavior. This has been previously attributed to the highly polarized host ce [8]. In order to correlate the T dependence of the Gd^{3+} g shift in $GdFe_2Zn_{20}$ with the highly polarized host ce [magnetic susceptibility for YFe_2Zn_{20} (χ_Y)], Fig. 6 presents the T dependence of $(H^T - H^{150}_{3620})/H^{150}$ and $-\chi_Y$, where H^{150}_{3620} is the highest-T (150 K) resonance field (3620 Oe) that was measurable for the Gd^{3+} resonance in $GdFe_2Zn_{20}$. It is worth mentioning that this T dependence of $H_{\rm res}$ is still observable even in samples with highly diluted Gd^{3+}, such as $Y_{0.95}Gd_{0.05}Fe_2Zn_{20}$ (not shown here).

Since $g_{\rm eff} \propto g[1 + \lambda\chi_Y]$ is equivalent to $(H^T - H^{150})/H^{150}_{3620} \propto \lambda\chi_Y$ [24], remembering the resonance condition $h\nu = g\mu_B H_0$, the observed correlation in Fig. 6 allows us to roughly estimate $\lambda = -12.5(5)$ mol Oe/emu for the molecular field parameter due to the polarized nature of the host itinerant d-like ce YFe_2Zn_{20}. In terms of the exchange interaction J_0, we can use the fact that $\lambda\,\chi_P = J_0(\eta_F/n)$ within the itinerant molecular field model [25]. In order to evaluate J_0, an adequate value of χ_P is required. Jia *et al.* [8] report a value of $\chi_{0\text{-dia}} = 5.96 \times 10^{-3}$ emu/mol Oe (low-T value) as the enhanced Pauli-like susceptibility for YFe_2Zn_{20} and a Stoner parameter of $\alpha = 0.88$ using the value of their Sommerfeld coefficient. Recalling that the Pauli susceptibility is temperature independent, we instead adopt the high-T value (after discounting the core diamagnetic contribution) $\chi_{0\text{-dia}} = 1.46 \times 10^{-3}$ emu/mol Oe (see the inset of Fig. 4) which gives a Stoner parameter of $\alpha = 0.51$. With this in mind, an appropriate Pauli susceptibility without enhancement is $\chi_{0\text{-dia}} \times (1 - 0.51) = \chi_P = 0.71 \times 10^{-3}$ emu/mol Oe. Thus, using this value for χ_P, plus $n = 23$ atoms/f.u. and $\eta_F = 21.2$ states/eV f.u. (in accordance with C_p measurements for YFe_2Zn_{20} [8]), we estimate the exchange parameter associated with the T-dependent itinerant molecular field as $J_0 = -9.7(4)$ meV. This is comparable to the reported value by Jia *et al.* [7] ($|J_0| \approx 4$ meV) obtained by applying the s-d model in the case of $Gd_xY_{1-x}Fe_2Zn_{20}$.

Hence, these results indicate that the T dependence of the effective g value $g_{\rm eff}$ is in fact associated with an internal AFM molecular field arising from the highly polarized, itinerant, d-like ce. It is also associated with the intrinsic g shift caused by the exchange interaction between the Gd^{3+} localized magnetic moment and the d-like ce.

With the aim of estimating the exchange parameters in a more traditional way by using the ESR analysis (in order to obtain more physical information), we now explore the high-T region, that shows only a minor T dependence and in which the formalism works well. Therefore, hereafter we shall use the high-T g shift instead of $g_{\rm eff}$. The exchange interaction

TABLE II. Partial density of states at the Fermi level for YFe_2Zn_{20} and $GdFe_2Zn_{20}$ (states/eV f.u. spin) with the associated *ce* polarization: spin up (↑) and spin down (↓).

Ion	*s* like	*p* like	*d* like	*f* like
Y	0.0010 ↑ 0.0035 ↓	0.0051 ↑ 0.0042 ↓	0.1017 ↑ 0.0803 ↓	
Fe	0.0037 ↑ 0.0021 ↓	0.0180 ↑ 0.0110 ↓	1.8469 ↑ 0.5748 ↓	
Zn	0.1575 ↑ 0.0747 ↓	0.71535↑ 0.3292 ↓	0.3116 ↑ 0.1306 ↓	
Gd	0.0035 ↑ 0.0007 ↓	0.0110 ↑ 0.0037 ↓	0.1447 ↑ 0.0950 ↓	0.0360 ↑ 0.0070 ↓
Fe	0.0038 ↑ 0.0048 ↓	0.0381 ↑ 0.0150 ↓	0.8803 ↑ 1.9918 ↓	
Zn	0.1834 ↑ 0.1644 ↓	0.7298 ↑ 0.7981 ↓	0.2623 ↑ 0.3477 ↓	

$\mathcal{H} = -J_{fd}\vec{S}_f \cdot \vec{s}_{ce}$ between the localized $4f$-electron spin of Gd^{3+}, $\vec{S}_f$, and the *ce* of $GdFe_2Zn_{20}$, $\vec{s}_{ce}$, yields an ESR g shift Δg [26] and thermal broadening of the linewidth b (Korringa rate) [27] given by

$$\Delta g = J_{f.ce}(0)\eta_F \tag{1}$$

and

$$b = \frac{d(\Delta H)}{dT} = \frac{\pi k_B}{g\mu_B} J_{f.ce}^2(0)\eta_F^2 = \frac{\pi k_B}{g\mu_B}(\Delta g)^2, \tag{2}$$

where $J_{f.ce}(0)$ is the effective exchange parameter in the absence of *ce* momentum transfer, i.e., $\langle J_{f.ce}(q)\rangle_F = J_{f.ce}(0)$ [12], η_F is the "bare" density of states at the Fermi surface, k_B is the Boltzmann constant, μ_B is the Bohr magneton, and g is the Gd^{3+} g value. Using the ESR g shift, $\Delta g \approx -0.13$, for $GdFe_2Zn_{20}$ [$H_{3620}^{150} = 3620$ Oe $\rightarrow g = 1.864(2)$] in Eq. (2) we obtain $b \cong 388$ Oe/K, which is too large when compared with our experimentally measured value of $b = 14.4(7)$ Oe/K (see Fig. 1). This indicates that for $GdFe_2Zn_{20}$ we must use a single band description of the microscopic parameters [28], contrary to the multiband case of YCo_2Zn_{20} [4]. It also indicates that there is a strong *ce* momentum transfer dependence of the exchange parameters, i.e., $\langle J_{fd}(q)\rangle_F \neq J_{fd}(0)$, due to the possible change of the Fermi surface [13]. Additionally, based on specific heat measurements and dc magnetic susceptibility [7,8], it is reasonable to assume a strong electron-electron correlation of the d-like *ce* and a high density of states at the Fermi level that must be taken into consideration in our calculations. Therefore, the two previous ESR equations must include such an electron-electron correlation term, and become

$$\Delta g = \frac{J_{fd}(0)\eta_{Fd}}{1-\alpha_d} \tag{3}$$

and

$$b = \frac{\pi k_B}{g\mu_B}\left[F_d \frac{\langle J_{fd}^2(q)\rangle_F \eta_{Fd}^2}{(1-\alpha_d)^2} K(\alpha_d)\right], \tag{4}$$

where we adopt our estimated Stoner parameter $\alpha = 0.51$ (instead of $\alpha = 0.88$ [8] for YFe_2Zn_{20}) and a single band description (mainly d-like at the Fermi level; see Fig. 5). Here, $\langle J_{fd}(q)\rangle_F$ is the average over the Fermi surface of the exchange parameter between the $4f$ and d-like *ce* involving the *ce* momentum transfer, α_d the Stoner parameter (assuming the electron-electron correlation just for the d-like *ce*), $K(\alpha_d)$ the reduction factors of the Korringa relaxation for core polarization [29,30], and $F_d = \frac{1}{5}$ a factor associated with the orbital degeneracy of the unsplit (no crystal-field effects) bands at the Fermi level. Thus, using $\Delta g = -0.13(4)$ (high-T, low-T dependence internal AFM molecular field), $b = 14.4(7)$ Oe/K [see Fig. 1(a)], $\eta_{Fd} = 3.05(1)$ states/eV f.u. (from our DFT calculations), $\alpha = 0.51$, $K(\alpha) = 0.6063$ [29,30] for $GdFe_2Zn_{20}$ in Eqs. (3) and (4), we estimate $J_{fd}(0) = -20(6)$ meV and $\langle J_{fd}(q)\rangle_F = 11.4(6)$ meV. It is worth noting that the obtained values are comparable to those from the method described in Fig. 6. The negative value for the $q = 0$ component of the exchange parameter [$J_{fd}(0) < 0$] indicates that the nature of the exchange coupling has changed to covalentlike as the Fe ions were incorporated into the lattice (d-band filling) as our DFT calculations showed for $y = 0.25$, 0.5, and 0.75. Notice that for $GdCo_2Zn_{20}$ [4] it is expected to be positive [$J_{fd}(0) > 0$] due to the ioniclike nature of the exchange coupling associated with the *ce* occupancy of the Gd $5d$ virtual bound states [12]. This covalent coupling, actually AFM, between the Gd^{3+} $4f$ and d-like *ce* suggests that the FM coupling between the Gd^{3+} ions in $GdFe_2Zn_{20}$ should be processed through a superexchangelike interaction via the d band of Fe orbitals, as illustrated in Fig. 7. The mechanism, which supports the ideas put forward by Jia *et al.* [8], contrasts strikingly with that for the AFM order of $GdCo_2Zn_{20}$, attributed to standard RKKY interactions via the s-like *ce* [4].

In addition to the experimental support for the coupling mechanism in the $GdFe_2Zn_{20}$, a broad scenario can be extracted from our ESR parameters by analyzing the complete evolution of the microscopic description (exchange interaction) starting from $GdCo_2Zn_{20}$. Figure 8 shows the evolution of the $b/(\Delta g)^2$ parameter as a function of the Fe concentration.

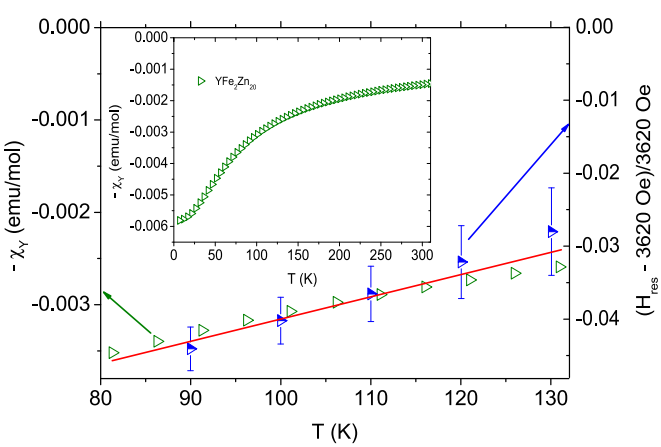

FIG. 6. Plots of $(H^T - H^{150})/H_{3620}^{150}$ (in $GdFe_2Zn_{20}$) and $-\chi_Y$ (in YFe_2Zn_{20}) vs T. See text for details.

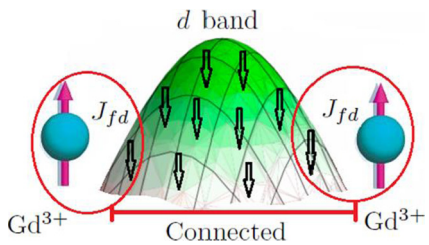

FIG. 7. Illustration of the Gd-Gd coupling mediated by the d-band conduction electrons and a negative coupling between Gd-(ce).

This parameter [see Eq. (2)] allows us to trace the crossover between the two regimes: $b/(\Delta g)^2 > 2.34 \times 10^4$ Oe/K for multiband and absence of q dependence of the exchange interaction and $b/(\Delta g)^2 < 2.34 \times 10^4$ Oe/K for a single band and q dependence of the exchange interaction [29,31,32]. Conspicuously, the crossover value of 2.34×10^4 Oe/K is attainable around $0.15 < y < 0.20$, which may correspond to the percolation limit for this material. It is enlightening to see the evolution of the Gd-Gd coupling from the point of view of a d-band filling in which the microscopic interaction is changed upon going from $GdCo_2Zn_{20}$ to $GdFe_2Zn_{20}$.

For completeness, Fig. 9 summarizes, in the form of an "extended phase diagram," both the Gd and the Fe substitutional evolution of the EPR parameters Δg and b going from the Pauli-like paramagnetic compound YCo_2Zn_{20} through the AFM compound $GdCo_2Zn_{20}$ and to the FM compound $GdFe_2Zn_{20}$.

In our previous ESR work [4] on the evolution of the ESR parameters in $Y_{1-x}Gd_xCo_2Zn_{20}$, it was shown that a multiband framework concomitant with an absence of a q dependence of the exchange interaction $\langle J_{fs}(q)\rangle_F = J_{fs}(0)$ gives the appropriate description of the exchange coupling between the Gd^{3+} localized magnetic moment and the band ce. Conversely, in the present work the Co substitution by Fe in $Gd(Co_{1-y}Fe_y)_2Zn_{20}$ changes the scenario dramatically after a percolation limit of the system is crossed. Within the new regime, both EPR parameters Δg and b feature dramatic deviations with Fe concentration. Δg becomes T dependent and presents and increasing negative shift toward higher T with the concomitant increase in b, showing the fundamental role of the d-band filling that allows the ESR data to be analyzed within a single d-band model. These results are consistent with the increase of the DOS at the Fermi level by the Fe substitution for Co, and supported by both our DFT calculations and by reported specific heat measurements [8].

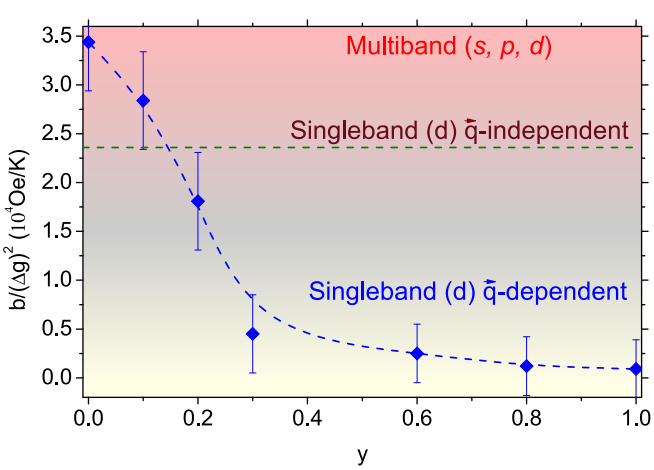

FIG. 8. Korringa-like parameter divided by the g-shift square $[b/(\Delta g)^2]$ as a function of y in $Gd(Co_{1-y}Fe_y)_2Zn_{20}$.

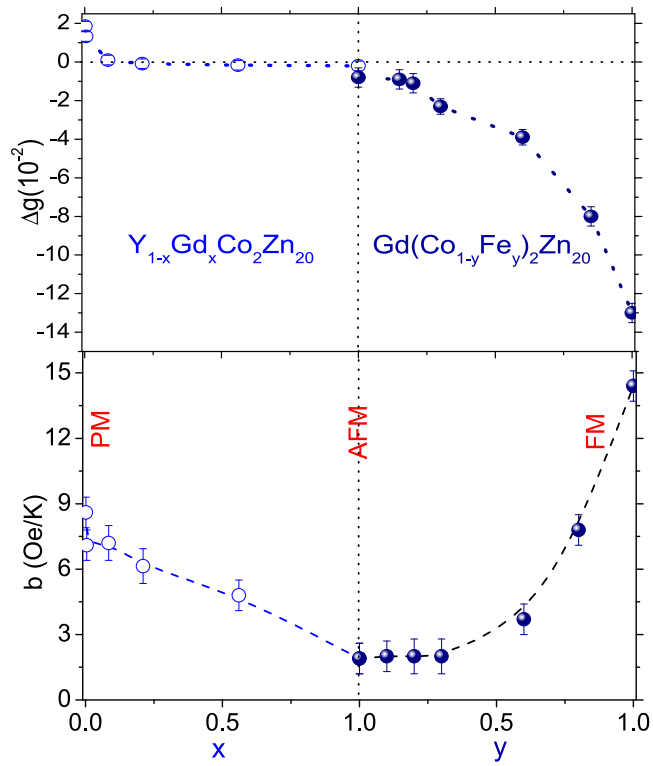

FIG. 9. Summary of the evolution of the ESR parameters (Δg and b) when going from a Pauli-like system (YCo_2Zn_{20}), passing through an antiferromagnetic state ($GdCo_2Zn_{20}$), and finally reaching a ferromagnetic system ($GdFe_2Zn_{20}$).

V. CONCLUSIONS

Our EPR results have shown that for the FM $GdFe_2Zn_{20}$ intermetallic compound there is a covalentlike exchange coupling [negative exchange parameter, $J_{fd}(0) < 0$] between the localized $4f$ electron of the Gd^{3+} ions and the d-like conduction electrons at the Fermi level. Furthermore, our results confirm a q dependence for the exchange parameter, i.e., $J_{fd}(0) \neq \langle J_{fd}(q)\rangle_F$. These experimental results suggest that a cloud of d-like ce polarized opposite to the Gd^{3+} magnetic moments should mediate and be the origin of the FM coupling between the Gd^{3+} ions. This scenario is also supported by our DFT calculations where a stable configuration is obtained when the Gd^{3+} $4f$ electrons are oppositely coupled to the d-like ce.

Finally, the results demonstrate unequivocally that the standard RKKY coupling mechanism, which was appropriate to describe the AFM order in the multiband uncorrelated ce system $GdCo_2Zn_{20}$, is not applicable to the FM order of $GdFe_2Zn_{20}$. Here, a single d band with a strong electron-

electron correlation (within the Stoner criteria) mediates a superexchangelike coupling between the Gd^{3+} magnetic moments. Therefore, we propose that the filling of the d band, above the percolation threshold of $y \gtrsim 0.3$, is responsible for the coupling mechanism and for the evolution from the low-T AFM order in $GdCo_2Zn_{20}$ to the high-T FM order in $GdFe_2Zn_{20}$.

ACKNOWLEDGMENTS

This work was supported by Brazilian agencies FAPESP (Grants No. 2011/19924-2 and No. 2012/17562-9), CNPq, FINEP, and CAPES. J.M.O.G. would like to thank CODI-Vicerrectoría de Investigación-Universidad de Antioquia (Estrategia de Sostenibilidad 2016-2017).

[1] X. Lin, V. Taufour, S. L. Bud'ko, and P. C. Canfield, Philos. Mag. **94**, 1277 (2014).
[2] W. M. Swift and W. E. Wallace, J. Solid State Chem. **3**, 180 (1971).
[3] K. H. J. Buschow, J. Less Common Met. **43**, 55 (1975).
[4] M. Cabrera-Baez, A. Naranjo-Uribe, J. M. Osorio-Guillén, C. Rettori, and M. A. Avila, Phys. Rev. B **92**, 214414 (2015).
[5] Y. Feng, J. Wang, D. M. Silevitch, B. Mihaila, J. W. Kim, J.-Q. Yan, R. K. Schulze, N. Woo, A. Palmer, Y. Ren, J. V. Wezel, P. B. Littlewood, and T. F. Rosenbaum, Proc. Natl. Acad. Sci. USA **110**, 3287 (2013).
[6] T. Moriya, *Spin Fluctuations in Itinerant Electron Magnetism* (Springer, Berlin, 1985).
[7] S. Jia, N. Ni, S. L. Bud'ko, and P. C. Canfield, Phys. Rev. B **76**, 184410 (2007).
[8] S. Jia, N. Ni, G. D. Samolyuk, A. Safa-Sefat, K. Dennis, H. Ko, G. J. Miller, S. L. Bud'ko, and P. C. Canfield, Phys. Rev. B **77**, 104408 (2008).
[9] S. Jia, S. L. Bud'ko, G. D. Samolyuk, and P. C. Canfield, Nat. Phys. **3**, 334 (2007).
[10] T. Nasch, W. Jeitschko, and U. C. Rodewald, Z. Naturforsch. B **52**, 1023 (1997).
[11] S. L. Bud'ko, T. Kong, X. Ma, and P. C. Canfield, J. Phys.: Condens. Matter **27**, 336003 (2015).
[12] D. Davidov, K. Maki, R. Orbach, C. Rettori, and E. P. Chock, Solid State Commun. **12**, 621 (1973).
[13] M. Cabrera-Baez, A. Naranjo-Uribe, J. M. Osorio-Guillén, C. Rettori, and M. A. Avila (unpublished).
[14] R. A. Ribeiro and M. A. Avila, Philos. Mag. **92**, 2492 (2012).
[15] P. C. Canfield and Z. Fisk, Philos. Mag. **65**, 1117 (1992).
[16] G. Kresse and J. Furthmüller, Phys. Rev. B **54**, 11169 (1996).
[17] G. Kresse and D. Joubert, Phys. Rev. B **59**, 1758 (1999).
[18] J. P. Perdew, A. Ruzsinszky, G. I. Csonka, O. A. Vydrov, G. E. Scuseria, L. A. Constantin, X. Zhou, and K. Burke, Phys. Rev. Lett. **100**, 136406 (2008).
[19] A. Abragam and B. Bleaney, *Electron Paramagnetic Resonance (EPR) of Transition Ions* (Clarendon, Oxford, U.K., 1970).
[20] G. Feher and A. F. Kip, Phys. Rev. **98**, 337 (1955).
[21] F. J. Dyson, Phys. Rev. **98**, 349 (1955).
[22] M. Cabrera-Baez, W. Iwamoto, E. T. Magnavita, J. M. Osorio-Guillén, R. A. Ribeiro, M. A. Avila, and C. Rettori, J. Phys.: Condens. Matter **26**, 175501 (2014).
[23] N. Ni, S. Jia, G. D. Samolyuk, A. Kracher, A. S. Sefat, S. L. Bud'ko, and P. C. Canfield, Phys. Rev. B **83**, 054416 (2011).
[24] J. G. S. Duque, E. M. Bittar, C. Adriano, C. Giles, L. M. Holanda, R. Lora-Serrano, P. G. Pagliuso, C. Rettori, C. A. Pérez, Rongwei Hu, C. Petrovic, S. Maquilon, Z. Fisk, D. L. Huber, and S. B. Oseroff, Phys. Rev. B **79**, 035122 (2009).
[25] J. M. D. Coey, *Magnetism and Magnetic Materials* (Cambridge University Press, Cambridge, U.K., 2009).
[26] K. Yosida, Phys. Rev. **106**, 893 (1957).
[27] J. Korringa, Physica **16**, 601 (1950).
[28] D. Davidov, R. Orbach, C. Rettori, D. Shaltiel, L. J. Tao, and B. Ricks, Phys. Lett. A **35**, 339 (1971).
[29] A. Narath, Phys. Rev. **163**, 232 (1967).
[30] R. W. Shaw and W. W. Warren, Phys. Rev. B **3**, 1562 (1971).
[31] D. Davidov, A. Chelkowski, C. Rettori, R. Orbach, and M. B. Maple, Phys. Rev. B **7**, 1029 (1973).
[32] T. Moriya, J. Phys. Soc. Jpn. **18**, 516 (1963).